EUMETSAT Satellite Application Facility on Climate Monitoring

Algorithm Theoretical Basis Document

UTH Edition 1.0

Upper Tropospheric Humidity TCDR **CM-14711**

Reference Number:	SAF/CM/UKMO/ATBD/UTH
Issue/Revision Index:	1.3
Date:	20.09.2019

Document Signature Table

	Name	Function	Signature	Date
Author	Viju John	CM SAF scientist		20.12.2018
Editor	Christoforos Tsamalis	CM SAF scientist		20.12.2018
Editor	Lizzie Good	CM SAF IBM		20.12.2018
Review	Rainer Hollmann	CM SAF Science Coordinator		05.01.2019
Approval	Steering Group			04.12.2018
Release	Martin Werscheck	Project Manager		10.01.2019

Distribution List

Internal Distribution	
Name	**No. Copies**
DWD Archive	1
CM SAF Team	1

External Distribution		
Company	**Name**	**No. Copies**
PUBLIC		1

Document Change Record

Issue/ Revision	Date	DCN No.	Changed Pages/Paragraphs
1.0	29.06.2016	SAF/CM/UKMO/ATBD/UTH/1.0	First version for review
1.1	29.07.2018	SAF/CM/UKMO/ATBD/UTH/1.1	Update after PCR
1.2	20.12.2018	SAF/CM/UKMO/ATBD/UTH/1.2	Final Editing and correction of reference to FCDR.
1.3	20.09.2019	SAF/CM/UKMO/ATBD/UTH/1.3	Missing References added (page 7, page 9)

Applicable Documents

Reference	Title	Code / Date
AD 1	Agreement between the European Organisation for the Exploitation of Meteorological Satellites (EUMETSAT) and the Federal Republic of Germany represented by the Deutsche Wetterdienst on the Continuous Development and Operations Phase of a EUMETSAT Satellite Application Facility in Climate Monitoring	1. December 2006

Reference Documents

Reference	Title	Code
RD 1	ERACLIM2-D3.11 - Microwave Humidity Sounder Radiance Data Record, v1B Draft, 10 August 2017 (available from www.era-clim2.eu/products under D3.11)	EUM/OPS/TEM/17/926984
RD 2	CM SAF Product Requirements Document	SAF/CM/DWD/PRD/2.10
RD 3	CM SAF Upper Tropospheric Humidity (UTH) Edition 1.0 Validation Report	SAF/CM/UKMO/VAL/UTH/1.1

Table of Contents

List of Tables

List of Figures

1 The EUMETSAT SAF on Climate Monitoring (CM SAF)

The importance of climate monitoring with satellites was recognized in 2000 by EUMETSAT Member States when they amended the EUMETSAT Convention to affirm that the EUMETSAT mandate is also to “contribute to the operational monitoring of the climate and the detection of global climatic changes". Following this, EUMETSAT established within its Satellite Application Facility (SAF) network a dedicated centre, the SAF on Climate Monitoring (CM SAF, http://www.cmsaf.eu).

The consortium of the CM SAF currently comprises the Deutscher Wetterdienst (DWD) as host institute, and the partners from the Royal Meteorological Institute of Belgium (RMIB), the Finnish Meteorological Institute (FMI), the Royal Meteorological Institute of the Netherlands (KNMI), the Swedish Meteorological and Hydrological Institute (SMHI), the Meteorological Service of Switzerland (MeteoSwiss), and the Met Office, the Meteorological Office of the United Kingdom. Since the beginning in 1999, the EUMETSAT CM SAF has developed and will continue to develop capabilities for a sustained generation and provision of Climate Data Records (CDRs) derived from operational meteorological satellites.

In particular the generation of long-term data records is pursued. The ultimate aim is to make the resulting data records suitable for the analysis of climate variability and potentially the detection of climate trends and validation of climate models and reanalyses. This will serve to improve climate model predictions at both global and regional scales. The CM SAF works in close collaboration with the EUMETSAT Central Facility and liaises with other satellite operators to advance the availability, quality and usability of Fundamental Climate Data Records (FCDRs) as defined by the Global Climate Observing System (GCOS). As a major task, the CM SAF utilizes FCDRs to produce records of Essential Climate Variables (ECVs) defined by GCOS. Thematically, the focus of CM SAF is on ECVs associated with the global energy and water cycle.

Another essential task of CM SAF is to produce data records that can serve applications related to the new Global Framework of Climate Services initiated by the WMO World Climate Conference-3 in 2009. The CM SAF supports climate services at national meteorological and hydrological services (NMHSs) with long-term data records but also with data sets produced close to real time that can be used to prepare monthly/annual updates of the state of the climate. Both types of products together allow for a consistent description of mean values, anomalies, variability and potential trends for the chosen ECVs. The new Copernicus Climate Change Service being set up by the European Union is another important customer for the CM SAF data records.

As an essential partner in the related international frameworks the CM SAF assumes the role of the main implementer of EUMETSAT’s commitments in support of global climate monitoring. This is achieved through:

- Application of the highest standards and guidelines as prescribed by GCOS for the satellite data processing,

- Processing of satellite data within an international collaboration whose participants benefit from developments at international level and pollinate the partnership with their own ideas and standards.
- Intensive validation and improvement of the CM SAF climate data records,
- Taking a major role in data record assessments performed by research organisations such as WCRP (World Climate Research Program),
- Maintaining and providing an operational and sustained infrastructure that can serve the community within the transition of mature CDR products from the research community into operational environments.
- Linking the products with the new climate services activities.

A catalogue of all available CM SAF products is accessible via the CM SAF webpage, www.cmsaf.eu.

2 Introduction

The aim of this document is to describe the algorithm theoretical basis of the upper tropospheric humidity (UTH) product from microwave humidity sounding measurements. Soden and Bretherton (1993) showed that measurements in a water vapour channel which probes the upper troposphere are approximately linearly dependent on the logarithm of the Jacobian weighted upper-tropospheric relative humidity (RH), hereafter referred to as UTH. Although it was derived for a specific infrared channel, the physical reasons are general (Ingram, 2010) and apply to any satellite instrument which responds primarily to upper-tropospheric humidity. At microwave frequencies, the upper tropospheric humidity channel is located at 183.31±1.00 GHz for the SSM/T-2, AMSU-B, and MHS instruments. These instruments have been in orbit since 1992 and are planned to continue for decades through instruments such as ATMS on NPP/JPSS and MWS on EPS-SG, thus providing a time series of more than 20 years of tropospheric data potentially available to the community for climate monitoring.

The main advantage of microwave based UTH is the availability of almost all-sky data, whereas infrared data sample only clear-sky areas (John et al., 2011). Microwave-based UTH was first introduced by Spencer and Braswell (1997). They used two months (January and July of 1994) of SSM/T-2 data to study the dryness of the tropical free troposphere. Buehler and John (2005) adapted the method for AMSU-B radiances and later a UTH data record was derived from AMSU-B and MHS measurements which is described in Buehler et al. (2008). The product described in this ATBD can be considered to a certain extent as a major update to the Buehler et al. (2008) data record. The main changes and improvements are highlighted and described below.

The new data record is based on a microwave humidity sounder FCDR) generated by EUMETSAT within the framework of the ERA-Clim2 project [RD 1]. By definition, a FCDR is a time series of level-1 satellite data (e.g., radiance, reflectance) which are corrected for non-climatic signals in the original measurements.

An improved retrieval scheme is tested and implemented for the estimation of UTH. UTH is Jacobian weighted relative humidity in the upper troposphere. Buehler and John (2005) used Jacobians in fractional volume mixing ratio (VMR) for their retrieval. It was later found that relative humidity (RH) Jacobians will result in a smaller retrieval error (Brogniez et al., 2004, Brogniez and Pierrehumbert (2007), and Brogniez et al., 2009). Procedures in Buehler and John (2005) will be followed in this ATBD, but using the RH Jacobian.

The addition of a daily UTH layer, which is the combination of ascending and descending layers. This has been introduced in order to minimize the impact of the UTH diurnal cycle due to orbit drift of the NOAA satellites (e.g. Chung et al., 2013).

3 Data and methods

3.1 Input Satellite data

The instruments of concern here are cross-track scanning passive total power microwave radiometers intended for humidity sounding (surface to 200 hPa), with three channels in the 183 GHz water vapour line but at different distances from its centre. In addition, two channels in the atmospheric "window" at lower frequencies are used primarily for cloud clearing and quality control. They are on notionally sun-synchronous polar-orbiting satellites: three are AMSU-B instruments (all on NOAA-series satellites) and three are MHS instruments (one on NOAA-18 satellite, two on MetOp-series satellites). Both AMSU-B and MHS form part of the “ATOVS” package starting in 1998 with the launch of NOAA-15. MHS is a follow-on instrument, first launched on NOAA-18 in 2005, to provide continuity of microwave UTH observations. Since the launch of NOAA-15 the measurements have been successfully assimilated in global and regional NWP models providing improvements to the representation of upper tropospheric humidity fields. There are 90 pixels across the scan for AMSU-B and MHS, with nadir footprint size of ~16 km, which increases away from nadir.

The particular input for the data record under consideration is the microwave humidity sounder FCDR generated by EUMETSAT within the framework of the ERA-Clim2 project [RD 1].

3.2 Radiative Transfer Model

The ARTS is a line-by-line radiative transfer model that simulates radiances from the infrared to the microwave spectral range (Buehler et al., 2006; Eriksson et al., 2011). The code is flexible from the user’s point of view and is freely available, along with comprehensive documentation (http://www.radiativetransfer.org/). The ARTS model has been validated against other models and satellite measurements (John and Buehler, 2005; Melsheimer et al., 2005; Buehler et al., 2006). PWR98 (Rosenkranz, 1998) for H_2O lines and continuum and PWR93 (Rosenkranz, 1993) for N_2 and O_2 lines and their respective continua are used to compute absorption coefficients. Furthermore, line data of O_3 was taken from the High Resolution Transmission (HITRAN) 2004 database (Rothman et al., 2003).

3.3 Retrieval method

As demonstrated in Buehler and John (2005), there is a simple linear relationship between radiances emanated from water vapour emissions in the upper troposphere (expressed in brightness temperature, T_b) and the natural logarithm of UTH, which is the Jacobian weighted relative humidity in the upper troposphere:

Equation 3-1

$$\ln(UTH) = a + b * T_b$$

The coefficients *a* and *b* are typically determined by linear regression, using a training data set of atmospheric temperature and humidity profiles. To get valid coefficients, the data set should capture the atmospheric variability as best as possible. To derive the coefficients in Equation 3-1, it is assumed that the relative humidity and the temperature lapse rate are constant in the upper troposphere, which is not true for realistic profiles. Long-term climate trends may also introduce subtle yet systematic changes in the error characteristics. Vertical structure will thus lead to violations of Equation 3-1, but the resulting errors will be included in the error analysis, if the error analysis is based on realistic profiles. A dataset developed by Chevallier et al. (2006) is used. This dataset is suitable for such purposes, because it contains many different atmospheric states, including common and extreme cases. It consists of diverse atmospheric profiles, selected from reanalysis of the European Centre for Medium-range Weather Forecasting (ECMWF). It will be referred to as the Chevallier dataset. The dataset consists of several collections of 5000 profiles, each selected to maximise variability in a particular parameter: temperature, humidity, ozone, cloud condensate and precipitation. In this ATBD, the collection which maximises the variability in humidity is used. As a result, retrieval error estimated using this dataset (see Section 3.4) might be conservative, i.e., probably larger than the "best estimate" of error.

Profiles of temperature, humidity, and ozone are used as inputs to ARTS (Eriksson et al., 2011) to produce brightness temperatures that would be seen by the microwave humidity sounder channels. In addition to brightness temperatures, Jacobians are also computed. The Jacobian at a particular level of the atmosphere represents the change in radiance per unit change in water vapour at that particular level. Jacobians of the 183.31±1.00 GHz channel are normally in a broad layer between 500 and 200 hPa, but the actual position of individual Jacobians varies according to the amount of water vapour. In a wetter atmosphere the Jacobians will peak at relatively higher altitudes, and in a drier atmosphere at relatively lower altitudes. In a very dry atmosphere, when the total column water vapour is less than about 3 mm, the Jacobians may include contributions from the surface and in such cases one cannot retrieve UTH from the measurements.

The UTH is defined as follows:

Equation 3-2

$$UTH = \frac{\sum_i RHi \cdot Wi}{\sum_i Wi}$$

where*, Wi* represents the water vapour Jacobian and *RHi* represents relative humidity at a particular vertical level in the troposphere. Jacobian can be defined in several ways. For example, Buehler and John (2005) computed the Jacobian based on water vapour VMR in fractional units. However, later studies have shown that for UTH retrieval, the Jacobian based on relative humidity (RH) is better suited (Schroeder et al., 2014; Brogniez et al., 2004, Brogniez and Pierrehumbert (2007), Brogniez et al., 2009, Moradi et al., 2015).

Figure 3-1 shows the relationship between ln(UTH) and 183.31±1.00 GHz channel brightness temperature for the two definitions of UTH using the Chevallier dataset. It is clear from Figure 3-1 that the UTH based on RH Jacobian shows higher linearity with the brightness temperatures compared with the UTH based on water vapour VMR Jacobian. Therefore, for the CM SAF data record, UTH is defined using the RH Jacobian. The

feasibility of a second order polynomial fit instead of a linear fit using the RH Jacobian was also explored, based on the following equation:

Equation 3-3

$$\ln(UTH) = a + b * T_b + c * T_b^2$$

Equation 3-3 provides the numerical values of the coefficients a, b and c used for each possible UTH retrieval. The CM-SAF UTH TCDR is produced based on the linear fit using the RH Jacobian; the justification for this choice is presented in the following section.

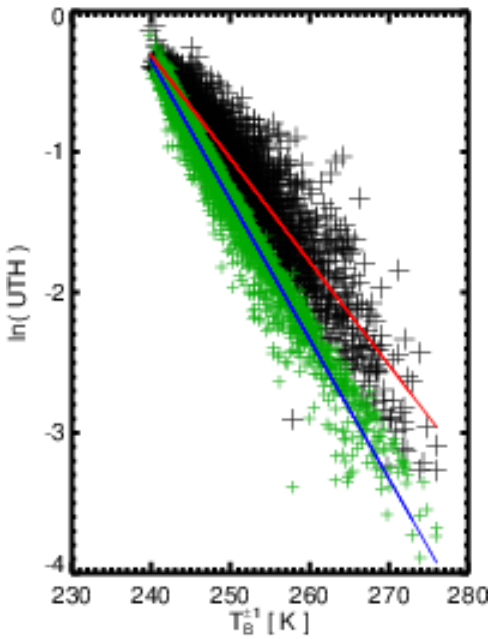

Figure 3-1: Logarithm of nadir UTH versus nadir brightness temperature of 183.31±1.00 GHz channel for the Chevallier et al. (2006) dataset. UTH is the channel's Jacobian weighted relative humidity in the upper troposphere. Black points represent UTH computed using volume mixing ratio (VMR) Jacobian and the green points represent UTH computed using relative humidity (RH) Jacobian. The red line represents a linear fit for the black points (correlation = -0.95) and the blue line represents a linear fit for the green points (correlation = -0.99).

Table 3-1: Fit parameters for possible UTH retrievals based on 183.31±1.00 GHz channel brightness temperatures using the VMR Jacobian and the RH Jacobian with linear regression and the RH Jacobian with 2nd order polynomial regression.

Retrieval	a	b	c
VMR Jacobian, linear fit	17.269384	-0.073271606	N/A
RH Jacobian, linear fit	23.467520	-0.099240916	N/A
RH Jacobian, 2nd order polynomial fit	57.983784	-0.37259756	0.00054075357

3.4 Error analyses

Figure 3-2 displays the bias and the standard deviation as a function of UTHtrue (i.e. from the simulations) for the three possible UTH retrievals. Figure 3-2 (top) shows the relative quantities, and Figure 3-2 (bottom) shows the absolute quantities. Retrieval statistics are computed by aggregating data points in 10% bins of the UTHtrue values. Absolute bias (Figure 3-2 – left bottom) is within approximately ±2% for UTH values below 60% for all retrieval methods. However, the retrievals using the RH Jacobian and the 2nd order polynomial fit show almost no bias below 50%. Above ~55% values all methods show a negative bias which reaches approximately -4% for the RH Jacobian linear-fit method. These results suggest using a 2nd order polynomial fit to minimise systematic biases in the UTH dataset, which is an essential requirement for a climate data record. For the 2nd order polynomial fit, the relative bias is within ±3% except for values between 0 and 10% where it increases to 7%. For the linear-fit RH Jacobian method the relative bias appears reasonably stable across the range of UTH values, and is within ±5% for all bins with the exception of the 60-70% where it is -6%. This in general meets the optimal requirement for UTH bias of ≤5%, as set out in the CM SAF PRD [RD 2]. It is assumed that retrieval biases contribute to the overall biases in the dataset because systematic biases in the measurements have already been removed as far as possible during the FCDR generation. This can only be verified when the final UTH dataset is validated against reference data [RD 3]. Relative biases are much higher for the VMR Jacobian method, reaching up to 30% for the 0-10% bin.

The standard deviation is significantly smaller for the RH Jacobian methods compared with the VMR Jacobian method for both the relative and absolute quantities (right-hand panels in Figure 3-2). The absolute standard deviation for the RH Jacobian methods increases approximately linearly from 1.5 to 3% for UTH values ranging from 0 to 30%, above which the values are quite stable. By contrast, the standard deviation for the VMR Jacobian method reaches a maximum of 5%, although it converges with the results from the RH Jacobian methods for the most extreme UTHtrue bins.

Although the RH Jacobian method with the second order polynomial fit results in a slightly reduced error compared to a linear fit, the linear fit method is used for the generation of CM SAF UTH product because there is a stronger physical basis for the linear fit as shown in Soden and Bretherton (1993) and Ingram (2010).

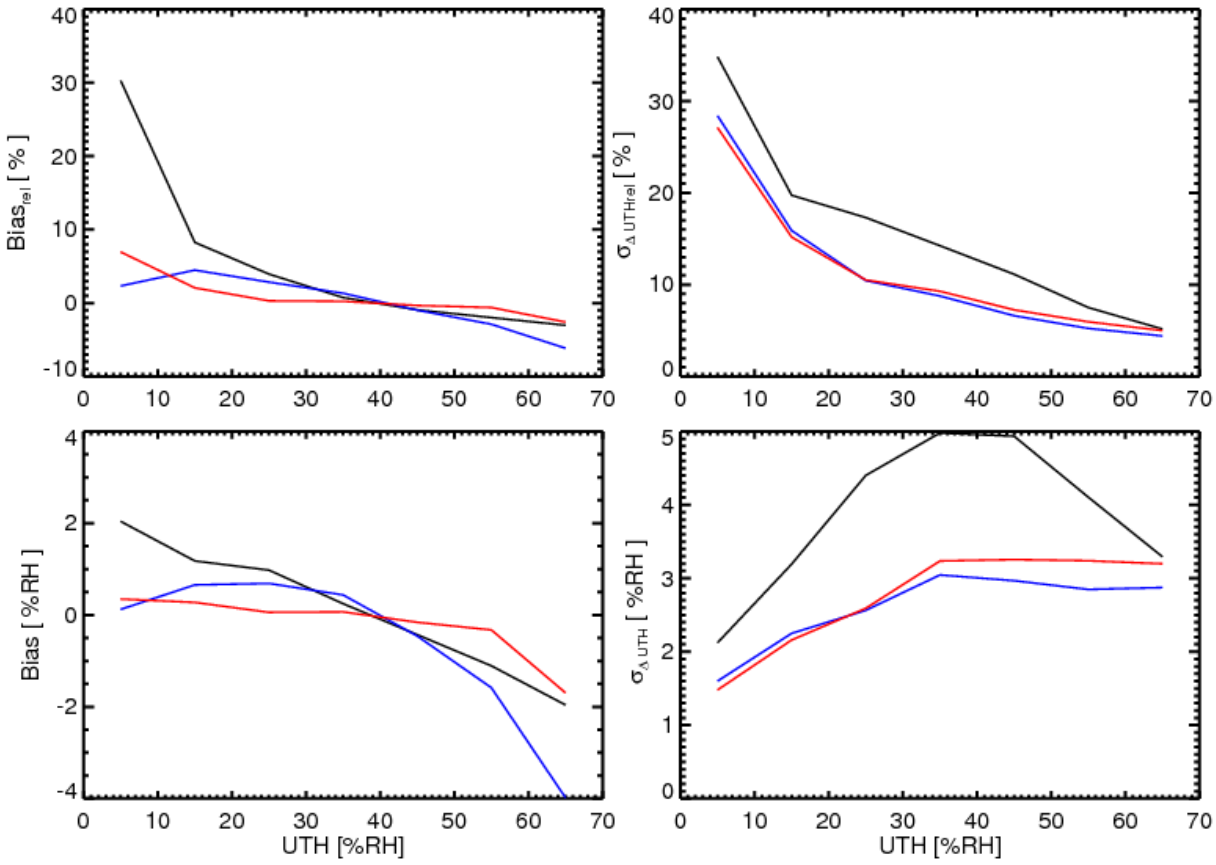

Figure 3-2: Bias (left) and standard deviation (right) of the three UTH retrievals against the true UTH (UTHtrue) from the simulations (abscissa). Top panels show the relative quantities, while the bottom panels the absolute quantities. Black lines represent retrieval based on UTH using VMR Jacobian, blue lines represent retrieval based on UTH using RH Jacobian, and red lines represent retrieval using RH Jacobian and a 2nd order polynomial fit.

4 Data processing

The production of the CM SAF UTH product includes some post-processing of the FCDR before applying the UTH retrieval, which is described below.

4.1 Removal of measurements contaminated by clouds

The influence of clouds on the propagation of electromagnetic waves is generally insignificant in the microwave spectrum, implying that radiance measurements of the 183-GHz water vapour absorption band are less prone to clear-sky sampling bias (e.g. John et al., 2011). However, the amount of radiation reaching space borne radiometers can be reduced because of scattering by large ice particles in the presence of deep convective or precipitating clouds (e.g. Greenwald and Christopher, 2002; Hong et al., 2005; Buehler et al., 2007). Therefore, cloud clearing methods are required to discard cloud-contaminated measurements that exhibit unreasonably low brightness temperatures.

Buehler et al. (2007) suggested an efficient method to remove cloud-contaminated measurements. The vertical distribution of weighting functions indicates that the 183.31±1 GHz channel is sensitive to higher levels in the troposphere than the 183.31±7 GHz (190.31 GHz for MHS) channel (e.g. Buehler and John, 2005). Because the atmospheric temperature generally decreases in the free troposphere, this means that brightness temperatures from the 183.31±1 GHz channel should be colder than those of the 183.31±7 GHz (190.31 GHz for MHS) channel under clear-sky conditions. However, such a relationship could be reversed in the presence of convective or precipitating clouds because of the scattering effects of ice particles or rain drops (Buehler et al., 2007; John et al., 2011). Therefore, a negative brightness temperature difference [i.e., 183.31±7 GHz − 183.31±1 GHz < 0] can be indicative of contamination by large ice particles or rain drops.

Radiative transfer simulations show that under clear-sky conditions, the computed 183.31±1 channel brightness temperature has a minimum value for each viewing angle. Because of the limb darkening effect, the brightness temperature decreases as the microwave radiometers scan away from the nadir. Since this minimum brightness temperature, which is a function of viewing angle, is considered to be warmer than the cloud-contaminated brightness temperature, a pre-computed table of the viewing-angle-dependent minimum brightness temperatures (Table 4-1, which is taken from Buehler et al. 2007) can be used as a tool for determining the cloud contamination in conjunction with the brightness temperature difference between the 183.31±7 GHz (190.31 GHz for MHS) and 183.31±1 GHz channels. The following two criteria suggested by Buehler et al. (2007) are applied to each measurement to identify cloud affected measurements, which are then discarded from further processing.

i. brightness temperature of the 183.31±1 GHz channel less than the viewing angle dependent threshold given in Table 4-1, and

ii. brightness temperature difference of the channels 183.31±7 (or 190.31 for MHS) GHz − 183.31±1 GHz less than 0 K.

Table 4-1: Viewing angle (θ in degrees from nadir) dependent threshold for the 183.31±1.00 GHz channel brightness temperature (T_b in K).

θ	T_b	θ	T_b	θ	T_b	θ	T_b	θ	T_b
0.55	240.1	10.45	239.8	20.35	239.2	30.25	238.0	40.15	236.4
1.65	240.1	11.55	239.8	21.45	239.2	31.35	238.0	41.25	236.1
2.75	240.1	12.65	239.7	22.55	239.1	32.45	237.8	42.35	235.8
3.85	240.1	13.75	239.7	23.65	239.0	33.55	237.6	43.45	235.5
4.95	240.1	14.85	239.6	24.75	238.8	34.65	237.4	44.55	235.2
6.05	240.1	15.95	239.6	25.85	238.7	35.75	237.2	45.65	234.9
7.15	240.1	17.05	239.5	26.95	238.6	36.85	237.0	46.75	234.4
8.25	239.9	18.15	239.4	28.05	238.5	37.95	236.7	47.85	233.9
9.35	239.9	19.25	239.3	29.15	238.3	39.05	236.6	48.95	233.3

4.2 Removal of measurements contaminated by surface

When total column water vapour is less than ~3 mm, the 183.31±1.00 GHz channel measurements are contaminated by surface emission and the UTH retrieval is no longer valid. Thus such measurements need to be removed before further processing. Under such dry conditions, the channel at 183.31±3.00 GHz already sees the surface due to the greater transparency of the atmosphere at this frequency compared to the 183.31±1.00 GHz, so both channels act as surface channels. In such cases, the 183.31±1.00 GHz channel will have higher brightness temperature than the 183.31±3.00 GHz channel due higher emissions from the atmosphere owing to the former's proximity to the water vapour line centre. Therefore, the condition 183.31±3.00 GHz − 183.31±1.00 GHz < 0 K is used to filter out surface contaminated measurements.

4.3 Limb correction

In addition to the cloud and surface filtering procedures, the limb darkening effect needs to be corrected for in order to make a temporally and spatially averaged data record from measurements with different satellite viewing angles. The scan angle dependence of observed brightness temperatures is generally adjusted by means of a linear multivariate regression. For the water vapour channels, however, an analytical relation can be employed to convert off-nadir brightness temperature ($T_b(\theta)$) into the nadir equivalent as follows (Chung et al., 2013):

Equation 4-1

$$T_b^{Nadir} = T_b(\theta) + \frac{\log(\cos\theta)}{d} T_b^{Nadir} = T_b(\theta) + \frac{\log(\cos\theta)}{d}$$

To determine d for the limb correction, brightness temperatures are simulated for a multitude of viewing angles (and thus satellite zenith angles) as well as the nadir case with atmospheric profiles of the 60-level sampled European Centre for Medium-Range Weather Forecasts (ECMWF) dataset

(Chevallier. 2001) as input to a radiative transfer model (Buehler et al., 2006). Figure 4-1 shows the brightness temperature difference between the off-nadir and nadir view cases for the 183.31 ± 1 GHz channel as a function of viewing angle. The vertical bars denote standard deviation at each viewing angle. As expected from the increased path for the off-nadir cases, the simulated brightness temperature is generally lower than for the nadir case. However, deviations from Equation 4-1

may occur because of surface influence or atmospheric temperature inversion in very dry conditions.

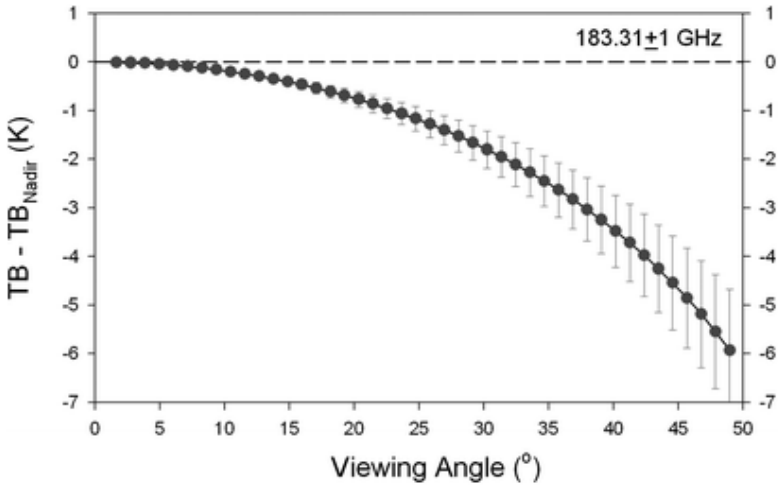

Figure 4-1: Brightness temperature difference from the nadir view case as a function of satellite viewing angle for the 183.31 ± 1 GHz channel. Closed circles and vertical bars denote mean and standard deviation, respectively. Brightness temperatures are simulated using atmospheric profiles of the Chevallier dataset (Figure taken from Chung et al., 2013).

Hence, these exceptional cases are excluded in the linear regression computations between the inverse of brightness temperature difference and log(cosθ). The computed value of d is −0.1045 for the 183.31±1.00 GHz channel.

4.4 Spatio-temporal averaging

The CM-SAF UTH product is provided to users on a global, daily 1.0° x 1.0° latitude-longitude grid. UTH is retrieved for all cloud and surface cleared and limb-corrected brightness temperatures for each day. These are then separated for ascending and descending passes and binned into each 1.0° grid cell, and the UTH cell mean, median, and standard deviation is computed. Information such as number of measurements used, number of measurements discarded due to cloud or surface contamination for every grid box is also provided. Statistics for the 183.31±1.00 GHz brightness temperature in each grid cell are included as an intermediate product in the dataset.

Without actively controlling the orbit (as done for MetOp satellites), the local equator crossing time (LECT) of a sun-synchronous satellite will slowly drift over its operational lifetime. Figure 4-2 shows the drift in LECT for the NOAA satellites, which are not actively controlled.

UTH has a diurnal cycle that closely follows the diurnal cycle of deep convection (e.g. Soden, 2000). The drifting orbits of the NOAA satellites will alias the diurnal cycle in the time-series

of UTH measurements (Chung et al., 2013; Kottayil et al., 2013). In order to account for orbital drift, a daily mean UTH is included in the CM SAF UTH data set, which is the weighted average of ascending and descending orbits for all grid cells with valid ascending and descending observations:

Equation 4-2

$$UTH_{daily} = \frac{N_{asc} * UTH_{asc} + N_{desc} * UTH_{desc}}{N_{asc} + N_{desc}}$$

where N stands for the number of UTH retrievals for ascending (asc) and descending (desc).

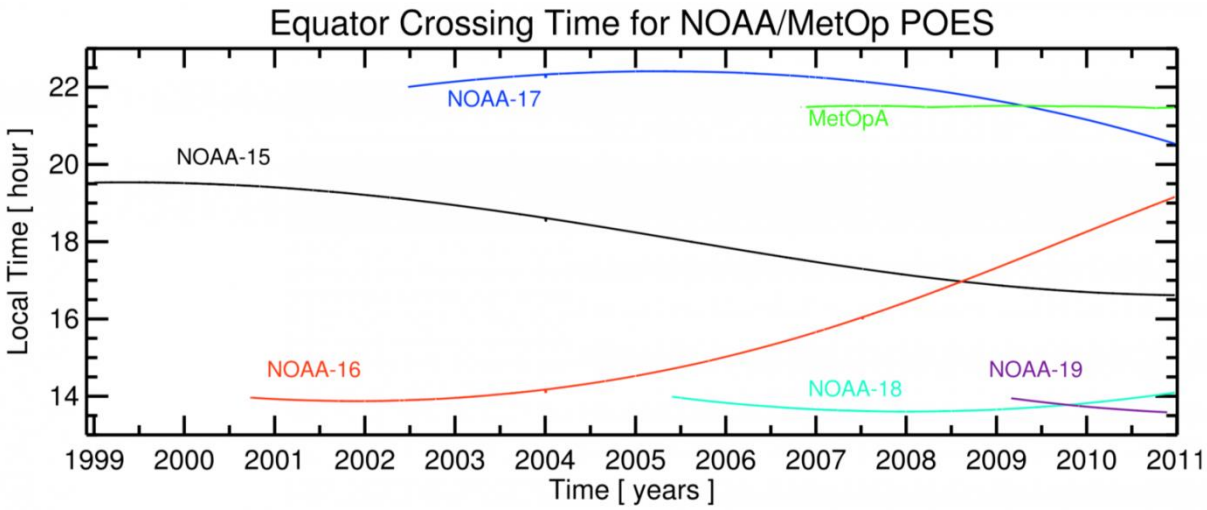

Figure 4-2: Equator crossing times of the ascending nodes of NOAA/MetOp sun synchronous satellites. Drifting of the orbits can be seen. MetOp-A is maintained in a stable orbit. Figure taken from John et al. (2012).

These daily gridded data, with includes both ascending and descending UTH fields and the daily mean UTH, are provided in NetCDF4 files. Figure 4-3 illustrates the different data processing steps for the production of the UTH data record.

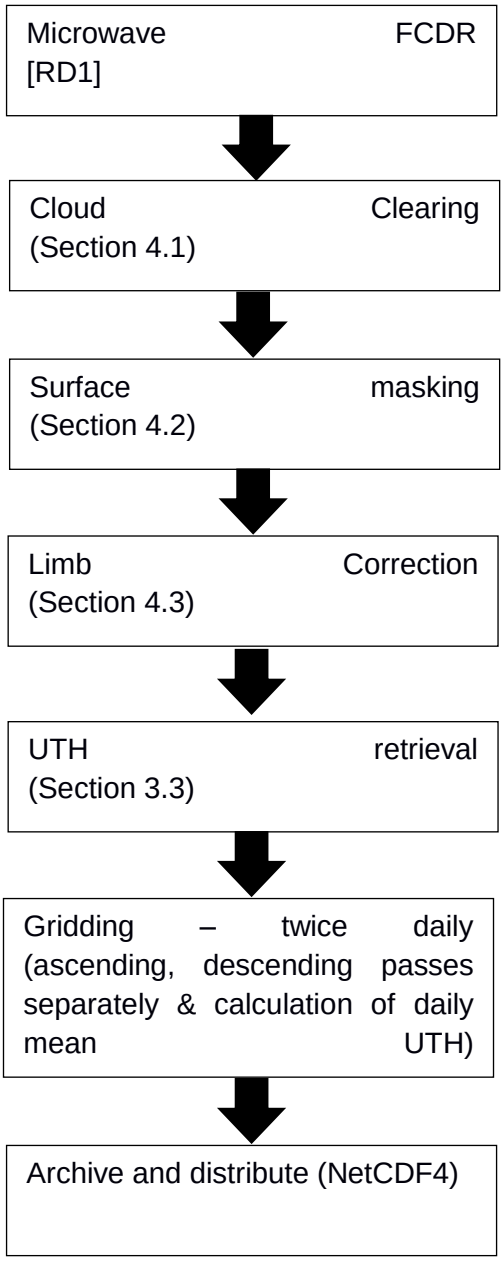

Figure 4-3: Steps involved in creation of the UTH data record.

5 Assumptions and limitations

The UTH retrieval method described here is a mere transformation of radiance, expressed in brightness temperature, measured by the 183.31±1.00 GHz channel to a more intuitive humidity unit. The relative humidity Jacobian which is used to define the UTH moves vertically depending on the water vapour load in the atmosphere. It is generally assumed that the Jacobian covers a broad atmospheric layer between 500 and 200 hPa. However, in a drier atmosphere the Jacobian will have significant contributions from altitudes below the 500 hPa level and in a wetter atmosphere there can be contributions from altitudes above the 200 hPa level. Therefore, the CM SAF UTH dataset should not be considered as an average relative humidity in a fixed vertical layer of the troposphere. Consequently it is not easy to compare this data record with other products, particularly water vapour profiles from radiosondes or model outputs. In order to obtain a like-to-like comparison, users should conduct radiative transfer simulations (for example with RTTOV or other fast radiative transfer models) using temperature and water vapour profiles from other sources (e.g. reanalyses, models, radiosondes) to obtain corresponding brightness temperatures and then perform an UTH retrieval as explained in Section 3.3 of this ATBD. There are several studies demonstrating this (e.g. Bodas-Salcedo et al., 2011; Chung et al., 2016).

The linear relationship between the natural logarithm of UTH and the 183.31±1.00 GHz measurements is derived based on the assumption that the lapse rate and relative humidity are uniform in the upper troposphere. Of course, the relative humidity in real profiles is far from uniform with height and this is reflected in the scatter between UTH and corresponding brightness temperatures (Figure 3-1). However, there is no physical basis for relative humidity to become more non-uniform in a warming climate. One potential issue is a changing lapse rate (e.g. Santer et al., 2005) due to amplification of the surface temperature trend in the tropical upper troposphere. On a multi-decadal time-scale this could be misinterpreted as systematic humidity changes in the upper troposphere.

The UTH retrieval is generally not valid outside ±60° latitude because of the very small amounts of water vapour in the upper troposphere. Therefore, data outside of this latitudinal range should be treated with caution by users. However, there will be a number of valid UTH retrievals outside ±60° latitude. Provided that there is no contamination from the surface, the humidity sounders will measure the relative humidity of the lower atmospheric layers using the 183.31±1.00 GHz channel, although not necessarily within the upper troposphere. Users can make informed decisions on the representativeness of the grid-point averages using the number of used and discarded measurements which are also provided in the dataset. However, it should be noted that evaluation of the CM SAF UTH product suggests that there is no accuracy dependence of the product on the number of observations used to calculate the grid-cell UTH [RD 3].

6 References

Bodas-Salcedo, A., M. J. Webb, S. Bony, H. Chepfer, J.-L. Dufresne, S. A. Klein, Y. Zhang, R. Marchand, J. M. Haynes, R. Pincus, and V. O. John (2011), COSP: satellite simulation software for model assessment, Bull. Amer. Met. Soc., 92, 1023–1043, doi:10.1175/2011BAMS2856.1.

Brogniez et al (2004), Interannual and intraseasonal variabilities of the free tropospheric humidity using METEOSAT water vapor channel over the tropics, EUMETSAT Meteorological Satellite Conference, Prague 31 May– 4 June.

Brogniez H., and R.T. Pierrehumbert (2007), Intercomparison of tropical tropospheric humidity in GCMs with AMSU-B water vapor data, GRL, 34, doi:10.1029/2006GL029118

Brogniez, H., R. Roca, and L. Picon, (2009), A study of the FTH interannual variability using Meteosat data and an advection-condensation transport model, J. Clim, 22, DOI: 10.1175/2009JCLI2963.1

Buehler, S. A. and V. O. John (2005), A Simple Method to Relate Microwave Radiances to Upper Tropospheric Humidity, J. Geophys. Res., 110, D02110, doi:10.1029/2004JD005111.

Buehler, S. A., N. Courcoux, and V. O. John (2006), Radiative transfer calculations for a passive microwave satellite sensor: Comparing a fast model and a line-by-line model, J. Geophys. Res., 111, D20304, doi:10.1029/2005JD006552.

Buehler, S. A., M. Kuvatov, T. R. Sreerekha, V. O. John, B. Rydberg, P. Eriksson, and J. Notholt (2007), A cloud filtering method for microwave upper tropospheric humidity measurements, Atmos. Chem. Phys., 7(21), 5531–5542, doi:10.5194/acp-7-5531-2007.

Buehler, S. A., M. Kuvatov, V. O. John, M. Milz, B. J. Soden, D. L. Jackson, and J. Notholt (2008), An Upper Tropospheric Humidity Data Set From Operational Satellite Microwave Data, J. Geophys. Res., 113, D14110, doi:10.1029/2007JD009314.

Chevallier, F. (2001), Sampled databases of 60-level atmospheric profiles from the ECMWF analysis, EUMETSAT SAF Program Res. Rep 4, Eur. Cent. for Medium-Range Weather Forecast., Reading, UK.

Chevallier F, Di Michele S, McNally AP. Diverse profile datasets from the ECMWF 91-level short-range forecasts (2006), Technical report, NWP SAF (Satellite Application Facility for Numerical Weather Prediction), Document no. NWPSAF-EC-TR-010, Version 1.0.

Chung, E.S., Soden, B.J. and John V.O. (2013), Intercalibrating Microwave Satellite Observations for Monitoring Long-Term Variations in Upper- and Midtropospheric Water Vapor, J. Atmospheric and Oceanic Technology, 30, 2303-2319, doi:10.1175/JTECH-D-13-00001.1

Chung, E.-S., B. J. Soden, X. L. Huang, L. Shi, V. O. John (2016), An assessment of the consistency between satellite measurements of upper tropospheric water vapor, Journal of Geophysical Research-Atmospheres, 121, 2874-2887.

Eriksson, P., S. A. Buehler, C. P. Davis, C. Emde, and O. Lemke (2011), ARTS, the atmospheric radiative transfer simulator, Version 2, J. Quant. Spectrosc. Radiat. Transfer, 112(10), 1551–1558, doi:10.1016/j.jqsrt.2011.03.001.

Greenwald, T. J., and S. A. Christopher (2002), Effect of cold clouds on satellite measurements near 183 GHz, J. Geophys. Res., 107(D13), doi: 10.1029/2000JD000258.

Hong, G., G. Heygster, J. Miao, and K. Kunzi (2005), Detection of tropical deep convective clouds from AMSU-B water vapor channels measurements, J. Geophys. Res., 110, D05205, doi: 10.1029/2004JD004949.

Ingram, W., (2010), A very simple model for the water vapour feedback on climate change. Q. J. R. Meteorol. Soc., 136, 30-40.

John, V. O., G. Holl, R. P. Allan, S. A. Buehler, D. E. Parker, and B. J. Soden (2011), Clear-sky biases in satellite infra-red estimates of upper tropospheric humidity and its trends, J. Geophys. Res., 116, D14108, doi:10.1029/2010JD015355.

John, V. O., G. Holl, S. A. Buehler, B. Candy, R. W. Saunders, and D. E. Parker (2012), Understanding inter-satellite biases of microwave humidity sounders using global simultaneous nadir overpasses, J. Geophys. Res., 117(D2), D02305, doi:10.1029/2011JD016349.

Kottayil, A., V. O. John, and S. A. Buehler (2013), Correcting diurnal cycle aliasing in satellite microwave humidity sounder measurements, J. Geophys. Res., 118(1), 101–113, doi:10.1029/2012JD018545.

Melsheimer, C., C. Verdes, S. A. Buehler, C. Emde, P. Eriksson, D. G. Feist, S. Ichizawa, V. O. John, Y. Kasai, G. Kopp, N. Koulev, T. Kuhn, O. Lemke, S. Ochiai, F. Schreier, T. R. Sreerekha, M. Suzuki, C. Takahashi, S. Tsujimaru, and J. Urban (2005), Intercomparison of General Purpose Clear Sky Atmospheric Radiative Transfer Models for the Millimeter/Submillimeter Spectral Range, Radio Sci., RS1007, doi:10.1029/2004RS003110.

Moradi, I., Ferraro, R. R., Soden, B. J., Eriksson, P., & Arkin, P. (2015), Retrieving Layer-Averaged Tropospheric Humidity from Advanced Technology Microwave Sounder Water Vapor Channels, IEEE Transactions on Geoscience and Remote Sensing, 53(12), 6675-6688, doi:10.1109/TGRS.2015.2445832.

Rosenkranz, P. W. (1993), Absorption of microwaves by atmospheric gases. Atmospheric Remote Sensing by Microwave Radiometry, M. A. Janssen, Ed., John Wiley and Sons, 37–90.

Rosenkranz, P. W. (1998) Water vapor microwave continuum absorption: A comparison of measurements and models. Radio Sci., 33, 919– 928; Corrigendum, 34, 1025

Rothman, L. S., and Coauthors (2003), The HITRAN molecular spectroscopic database: Edition of 2000 including updates through 2001, J. Quant. Spectrosc. Radiat. Transfer, 82, 5–44.

Santer, B.D., T.M.L. Wigley, C. Mears, F.J. Wentz, S.A. Klein, D.J. Seidel, K.E. Taylor, P.W. Thorne, M.F. Wehner, P.J. Gleckler, J.S. Boyle, W.D. Collins, K.W. Dixon, C. Doutriaux, M. Free, Q. Fu, J.E. Hansen, G.S. Jones, R. Ruedy, T.R. Karl, J.R. Lanzante, G.A. Meehl, V. Ramaswamy, G. Russell, and G.A. Schmidt (2005), Amplification of surface temperature trends and variability in the tropical atmosphere, Science, 309, 1551-1556, doi:10.1126/science.1114867.

Schröder, M., Roca, R., Picon, L., Kniffka, A., and Brogniez, H. (2014), Climatology of free-tropospheric humidity: extension into the SEVIRI era, evaluation and exemplary analysis, Atmos. Chem. Phys., 14, 11129-11148, doi:10.5194/acp-14-11129-2014.

Soden, B. J..and F. P. Bretherton (1993), Upper Tropospheric Relative Humidity From the GOES 6.7 µm Channel: Method and Climatology for July 1987, J. Geophys. Res., 98, 16,669-16,688.

Soden, B. J. (2000), The diurnal cycle of convection, clouds, and water vapour in the tropical upper troposphere, *Geophys. Res. Lett.* 27, 2173—2176.

R. W. Spencer and W. D. Braswell (1997), How Dry is the Tropical Free Troposphere? Implications for Global Warming Theory. Bull. Am. Met. Soc., 78, 1097-1106.

7 Glossary – List of Acronyms in alphabetical order

AMSU	Advanced Microwave Sounding Unit
ARTS	Atmospheric Radiative Transfer Model
ATBD	Algorithm Theoretical Basis Document
ATMS	Advanced Technology Microwave Sounder
CM SAF	Climate Monitoring Satellite Application Facility
DMSP	Defence Meteorological Satellite Program
ECMWF	European Centre for Medium Range Weather Forecast
ECV	Essential Climate Variable
EPS-SG	EUMETSAT Polar System – Second Generation
EUMETSAT	European Organisation for the Exploitation of Meteorological Satellites
FCDR	Fundamental Climate Data Record
GCOS	Global Climate Observing System
JPSS	Joint Polar Satellite System
METOP	Polar orbiting meteorological satellites operated by EUMETSAT
MHS	Microwave Humidity Sounder
NOAA	National Oceanic and Atmospheric Administration
NPP	National Polar-orbiting Partnership
RH	Relative Humidity
RTTOV	Radiative Transfer for TOVS
SSM/T2	Special Sensor Microwave Water Vapour Profiler
TCDR	Thematic Climate Data Record
TIROS	Television and Infrared Observation Satellite
TOVS	TIROS Operational Vertical Sounder
UTH	Upper Tropospheric Humidity
VMR	Volume Mixing Ratio
WCRP	World Climate Research Programme